Second-Order Nonlinear Optical Properties of Substituted Arylphosphine Oxides

Kevin L. Kott, Craig M. Whitaker, and Robert J. McMahon*

Department of Chemistry, University of Wisconsin, Madison, Wisconsin 53706-1396

Received November 18, 1994[⊗]

We report computational and experimental studies of the second-order nonlinear optical properties of substituted arylphosphine oxides (4-X-C_6H_4)Ph_2P=O (**1**), (4-X-C_6H_4)$_2$PhP=O (**2**), (4-X-C_6H_4)$_3$P=O (**3**) (where X = $-NH_2$ (**a**) and $-OH$ (**b**)), (4-$NH_2C_6H_4$)(4′-$NO_2C_6H_4$)PhP=O (**4**), and (4-$NH_2C_6H_4$)(4′-$CF_3C_6H_4$)$_2$P=O (**5**). Computational results (AM1/finite field and AM1/sum-over-states) predict that **1**, **2**, **4**, and **5** possess intrinsic molecular hyperpolarizabilities ($||\beta||$) comparable to 4-nitroaniline (**9**). Molecular orbital analysis indicates that the hyperpolarizability arises not by charge transfer from the donor group ($-NH_2$ or $-OH$) to the P=O moiety but instead by charge transfer from the donor group to the unsubstituted and/or acceptor-substituted aryl ring(s). This behavior is not well described by the "two-level model" of nonlinear optical response. The calculations indicate that the molecular hyperpolarizability and dipole moment are nearly orthogonal in **1** and **2**, greatly reducing the component of the molecular hyperpolarizability in the direction of the dipole moment (β_μ). Experimental measurements of β_μ using the technique of electric-field-induced second-harmonic generation (EFISH) reveal modest values for compounds **1**–**3** (β_μ ranging from 1.0×10^{-30} to 4.6×10^{-30} cm^5 esu^{-1}) in fairly good agreement with the calculations. EFISH measurements show phosphine oxides **4** and **5** have β_μ values (9.0×10^{-30} and 10.1×10^{-30} cm^5 esu^{-1}, respectively) twice as large as compounds **1**–**3** despite the fact that the intrinsic hyperpolarizabilities, $||\beta||$, of **4** and **5** are smaller. The increase in β_μ arises because the dipole moment vector in **4** and **5** is more nearly collinear with the major components of the hyperpolarizability tensor. Compounds **1**–**3** form highly crystalline solid-state structures characterized by extensive intermolecular hydrogen bonding and high thermal and mechanical stability. Experimental powder SHG results reveal that monosubstituted (**1a** and **1b**) and disubstituted (**4**) phosphine oxides are capable of second-harmonic generation (SHG) in the solid state (0.01, 1.0, and 1.0 × urea, respectively). X-ray crystal structures reveal that compounds **1a** and **1b** crystallize in the noncentrosymmetric space groups *Cc* and $Pca2_1$, respectively. Most importantly, the hyperpolarizability of phosphine oxides **1**–**3** and **5** arises in the absence of electronic absorptions in the visible spectral region; compounds **1**–**3** and **5** display excellent transparency (λ_{max} < 300 nm) in the visible and near-UV spectral regions.

The discovery of new organic materials exhibiting nonlinear optical response in combination with other desirable physical properties (optical transparency and thermal and mechanical stability) continues to be an important goal in nonlinear optics (NLO).[1–10] Typical organic NLO materials consist of a π-electron system (alkene, aromatic) substituted with an electron-donor and an electron-acceptor substituent.[8–10] Recent studies are beginning to provide a clearer understanding of the structural features responsible for nonlinear optical response in organic molecules. Experimental[11–23] and theoretical[24–31] investigations probed the relationship

[⊗] Abstract published in *Advance ACS Abstracts*, January 1, 1995.

(1) Eaton, D. F. *Science* **1991**, *253*, 281–287.
(2) Prasad, P. N.; Reinhardt, B. A. *Chem. Mater.* **1990**, *2*, 660–669.
(3) Williams, D. J. *Angew. Chem., Int. Ed. Engl.* **1984**, *23*, 690–703
(4) The interest in organic NLO materials derives from the potential use of these materials in diverse technological applications.[5–10]
(5) Kolinsky, P. V. *Opt. Eng.* **1992**, *31*, 1676–1684.
(6) Boyd, G. T. *J. Opt. Soc. Am. B* **1989**, *6*, 685–692.
(7) (a) Nayar, B. K.; Winter, C. S. *Opt. Quantum Electron.* **1990**, *22*, 297–318. (b) Assanto, G. *J. Mod. Opt.* **1990**, *37*, 855–873.
(8) *Nonlinear Optical Properties of Organic Molecules and Crystals*; Chemla, D. S., Zyss, J., Eds.; Academic Press: Orlando, FL, 1987.
(9) Prasad, P. N.; Williams, D. J. *Introduction to Nonlinear Optical Effects in Molecules and Polymers*; Wiley: New York, 1990.
(10) *Materials for Nonlinear Optics: Chemical Perspectives*; Marder, S. R., Sohn, J. E., Stucky, G. D., Eds.; ACS Symposium Series No. 455; American Chemical Society: Washington, DC, 1991.
(11) (a) Singer, K. D.; Sohn, J. E.; King, L. A.; Gordon, H. M.; Katz, H. E.; Dirk, C. W. *J. Opt. Soc. Am. B* **1989**, *6*, 1339–1350. (b) Katz, H. E.; Singer, K. D.; Sohn, J. E.; Dirk, C. W.; King, L. A.; Gordon, H. M. *J. Am. Chem. Soc.* **1987**, *109*, 6561–6563.
(12) (a) Cheng, L.-T.; Tam, W.; Stevenson, S. H.; Meredith, G. R.; Rikken, G.; Marder, S. R. *J. Phys. Chem.* **1991**, *95*, 10631–10643. (b) Cheng, L.-T.; Tam, W.; Marder, S. R.; Stiegman, A. E.; Rikken, G.; Spangler, C. W. *J. Phys. Chem.* **1991**, *95*, 10643–10652. (c) Stiegman, A. E.; Graham, E.; Perry, K. J.; Khundkar, L. R.; Cheng, L.-T.; Perry, J. W. *J. Am. Chem. Soc.* **1991**, *113*, 7658–7666. (d) Yuan, Z.; Taylor, N. J.; Marder, T. B.; Williams, I. D.; Kurtz, S. K.; Cheng, L.-T. *J. Chem. Soc., Chem. Commun.* **1990**, 1489–1492.
(13) (a) Marder, S. R.; Gorman, C. B.; Tiemann, B. G.; Cheng, L.-T. *J. Am. Chem. Soc.* **1993**, *115*, 3006–3007. (b) Tiemann, B. G.; Cheng, L.-T.; Marder, S. R. *J. Chem. Soc., Chem. Commun.* **1993**, 735–737. (c) Marder, S. R.; Cheng, L.-T.; Tiemann, B. G. *J. Chem. Soc., Chem. Commun.* **1992**, 672–674. (d) Marder, S. R.; Beretan, D. N.; Cheng, L.-T. *Science* **1991**, *252*, 103–106.
(14) Craig, G. S. W.; Cohen, R. E.; Schrock, R. R.; Silbey, R. J.; Puccetti, G.; Ledoux, I.; Zyss, J. *J. Am. Chem. Soc.* **1993**, *115*, 860–867.
(15) Jen, A. K.-Y.; Rao, V. P.; Wong, K. Y.; Drost, K. J. *J. Chem. Soc., Chem. Commun.* **1993**, 90–92.
(16) Suslick, K. S.; Chen, C.-T.; Meredith, G. R.; Cheng, L.-T. *J. Am. Chem. Soc.* **1992**, *114*, 6928–6930.
(17) Kelderman, E.; Derhaeg, L.; Heesink, G. J. T.; Verboom, W.; Engbersen, J. F. J.; van Hulst, N. F.; Persoons, A.; Reinhoudt, D. N. *Angew. Chem., Int. Ed. Engl.* **1992**, *31*, 1075–1077.
(18) Kawabe, Y.; Ikeda, H.; Sakai, T.; Kawasaki, K. *J. Mater. Chem.* **1992**, *2*, 1025–1031.

0897-4756/95/2807-0426$09.00/0

between molecular structure and molecular hyperpolarizability by studying different combinations of donor and acceptor substituents, altering the nature and the length of the intervening π system, and optimizing the combination of donor, acceptor, and intervening π system.

Our interest in phosphine oxides as second-order nonlinear optical materials stems from the fact that simple aromatic molecules containing the phosphine oxide group possess characteristics which may be highly desirable in certain applications. First, arylphosphine oxides exhibit significantly better optical transparency than aryl nitro compounds, because the electronic absorptions of phosphine oxides occur at shorter wavelength. Second, phosphine oxides are trifunctional electron acceptors, which means that they could be incorporated into extended structures. Conceptually, this approach is analogous to that of the sulfones.[21] The utility of the sulfone group in nonlinear optical materials arises not only from the polarity of an individual sulfone moiety, but the ability to combine many units in extended structures. Third, arylphosphine oxides form crystalline solids with desirable physical and mechanical properties and thus may be of use as cocrystallization aids in growing bulk second-order nonlinear optical crystals. Triphenylphosphine oxide (**6**) has been used previously as cocrystallization aid, owing to the strong hydrogen-bonding capability of the phosphoryl moiety.[32,33] Hydrogen bonding in the solid state can play a significant role in the formation of acentric crystals,

Scheme 1

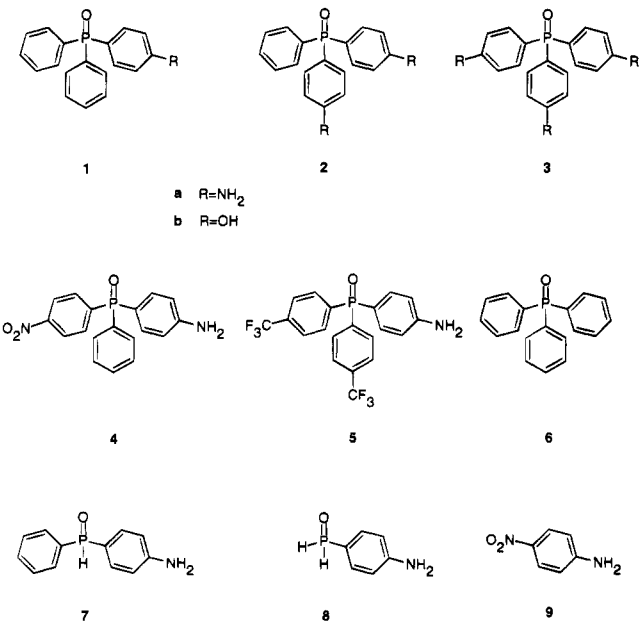

an important consideration in designing second-order nonlinear optical materials.[34,35] Substituted phosphine oxides such as **1**–**5** (Scheme 1) offer two possible advantages over the unsubstituted triphenylphosphine oxide (**6**): (i) The molecular hyperpolarizability of **6** is small; it cannot contribute significantly to the bulk nonlinear susceptibility, $\chi^{(2)}$, of the material. As a cocrystallization aid, **6** simply dilutes the nonlinearity of the sample. In contrast, **1**–**5** can contribute to the bulk nonlinear susceptibility of the material. (ii) Triphenylphosphine oxide (**6**) contains only a hydrogen bond acceptor group, whereas **1**–**5** contain both a hydrogen-bond donor and a hydrogen-bond acceptor. This presents the possibility that intermolecular hydrogen bonding in **1**–**5** could produce the desired head-to-tail alignment in the solid state.

In this paper, we address the central question of molecular hyperpolarizability in substituted phosphine oxides.[36] We report our computational (AM1/sum-over-states, AM1/finite field) and experimental (electric-field-induced second harmonic (EFISH) generation and powder second-harmonic generation) studies concerning the viability of the phosphine oxide (P=O, phosphoryl) substituent as an electron acceptor in second-order nonlinear optical materials.[33,37] Although the phosphine oxide moiety is a weaker electron acceptor than other substituents traditionally used in nonlinear optical (NLO) materials, recent studies indicate that the strong-

(19) (a) Puccetti, G.; Ledoux, I.; Zyss, J.; Jutland, A.; Amatore, C. *Chem. Phys.* **1992**, *160*, 467–475. (b) Barzoukas, M.; Blanchard-Desce, M.; Josse, D.; Lehn, J.-M.; Zyss, J. *Chem. Phys.* **1989**, *133*, 323–329.

(20) (a) Barzoukas, M.; Fort, A.; Klein, G.; Serbutoviez, C.; Oswald, L.; Nicoud, J. F. *Chem. Phys.* **1992**, *164*, 395–406. (b) Lequan, M.; Lequan, R. M.; Ching, K. C.; Barzoukas, M.; Fort, A.; Lahoucine, H.; Bravic, G.; Chasseau, D.; Gaultier, J. *J. Mater. Chem.* **1992**, *2*, 719–725.

(21) Ulman, A.; Willand, C. S.; Kohler, W.; Robello, D. R.; Williams, D. J.; Handley, L. *J. Am. Chem. Soc.* **1990**, *112*, 7083–7090.

(22) Huijts, R. A.; Hesselink, G. L. J. *Chem. Phys. Lett.* **1989**, *156*, 209–212.

(23) (a) Dulcic, A.; Flytzanis, C.; Tang, C. L.; Pepin, D.; Fetizon, M.; Hoppilliard, Y. *J. Chem. Phys.* **1981**, *74*, 1559–1563. (b) Dulcic, A.; Sauteret, C. *J. Chem. Phys.* **1978**, *69*, 3453–3457.

(24) (a) Kanis, D. R.; Ratner, M. A.; Marks, T. J. *Chem. Rev.* **1994**, *94*, 195–242. (b) Di Bella, S.; Fragala, I. L.; Ratner, M. A.; Marks, T. J. *J. Am. Chem. Soc.* **1993**, *115*, 682–686. (c) DeQuan, L.; Marks, T. J.; Ratner, M. A. *J. Phys. Chem.* **1992**, *96*, 4325–4336.

(25) (a) Matsuzawa, N.; Dixon, D. A. *J. Phys. Chem.* **1992**, *96*, 6232–6241. (b) Matsuzawa, N.; Dixon, D. A. *Int. J. Quantum Chem.* **1992**, *44*, 497–515.

(26) (a) Albert, I. D. L.; Pugh, D.; Morley, J. O.; Ramasesha, S. *J. Phys. Chem.* **1992**, *96*, 10160–10165. (b) Morley, J. O.; Pugh, D. *J. Chem. Soc., Faraday Trans.* **1991**, *87*, 3021–3025. (c) Morley, J. O.; Docherty, V. J.; Pugh, D. *J. Chem. Soc., Perkin Trans.* **1987**, 1351–1355.

(27) (a) Meyers, F. Brédas, J. L. *Synth. Met.* **1992**, *49–50*, 181–186. (b) Meyers, F.; Brédas, J. L.; Zyss, J. *J. Am. Chem. Soc.* **1992**, *114*, 2914–2921. (c) Brédas, J. L.; Meyers, F.; Pierce, B. M.; Zyss, J. *J. Am. Chem. Soc.* **1992**, *114*, 4928–4929. (d) Joffre, M.; Yaron, D.; Silbey, R. J.; Zyss, J. *J. Chem. Phys.* **1992**, *97*, 5607–5615. (e) Zyss, J.; Ledoux, I. *Chem. Rev.* **1994**, *94*, 77–106.

(28) Gao, X. L.; Feng, J. K.; Sun, C. C. *Int. J. Quantum Chem.* **1992**, *42*, 1747–1758.

(29) (a) Tsunekawa, T.; Yamaguchi, K. *J. Phys. Chem.* **1992**, *96*, 10268–10275. (b) Tsunekawa, T.; Yamaguchi, K. *Chem. Phys. Lett.* **1992**, *190*, 533–538.

(30) Barzoukas, M.; Fort, A.; Klein, G.; Boeglin, A.; Serbutoviez, C.; Oswald, L.; Nicoud, J. F. *Chem. Phys.* **1991**, *153*, 457–464.

(31) Dirk, C. W.; Twieg, R. J.; Wagniere, G. *J. Am. Chem. Soc.* **1986**, *108*, 5387–5395.

(32) Etter, M. C.; Baures, P. W. *J. Am. Chem. Soc.* **1988**, *110*, 639–640.

(33) Calvert, P. D.; Chaloner, P. A.; Corradi, M.; Harrison, R. M.; Hitchcock, P. B.; Rhodes, J. In *Organic Materials for Nonlinear Optics III*; Ashwell, G. J., Bloor, D., Eds.; *Spec. Publ. R. Soc.* **1993**, *137*, 118–123.

(34) (a) Etter, M. C.; Huang, K.-S. *Chem. Mater.* **1992**, *4*, 824–827. (b) Etter, M. C. *J. Phys. Chem.* **1991**, *95*, 4601–4610. (c) Etter, M. C.; Frankenbach, G. M.; Adsmond, D. A. *Mol. Cryst. Liq. Cryst.* **1990**, *187*, 25–39. (d) Etter, M. C.; Frankenbach, G. M. *Chem. Mater.* **1989**, *1*, 10–12. (e) Panunto, T. W.; Urbanczyk-Lipkowska, Z.; Johnson, R.; Etter, M. C. *J. Am. Chem. Soc.* **1987**, *109*, 7786–7797.

(35) (a) Zyss, J. *Adv. Mater.* **1993**, *5*, 120–123. (b) Zyss, J.; Nicoud, J. F.; Coquillay, M. *J. Chem. Phys.* **1984**, *81*, 4160–4167. (c) Zyss, J.; Berthier, G. *J. Chem. Phys.* **1982**, *77*, 3635–3653.

(36) Calvert et al. previously observed weak powder SHG from two chiral diaryl phosphine oxide derivatives. This study did not provide data concerning molecular hyperpolarizability.[33]

(37) Katz et al. utilized a phosphonate diester as a weak electron acceptor in a multilayer film that displayed second-harmonic generation: Katz, H. E.; Scheller, G.; Putvinski, T. M.; Schilling, M. L.; Wilson, W. L.; Chidsey, C. E. D. *Science* **1991**, *254*, 1485–1487. See also: Hutchings, M. G.; Gordon, P. F.; Duggan, P. J.; Ledoux, I.; Puccetti, G.; Zyss, J. *Tetrahedron Lett.* **1994**, *35*, 9073–9074.

est electron acceptor does not necessarily lead to the largest hyperpolarizability.[13] Our computational and experimental results establish that (4-aminophenyl)-diphenylphosphine oxide (**1a**) possesses a moderate intrinsic molecular hyperpolarizability, $||\beta||$, and that the hyperpolarizability and the dipole moment are nearly orthogonal to each other. The design of di- and trisubstituted compounds **4** and **5** includes simple changes in molecular structure to alter the relative orientation of $\boldsymbol{\mu}$ and $\boldsymbol{\beta}$, with the hope of exploiting the intrinsic hyperpolarizability of the monoaminophosphine oxide **1a**. This strategy was successful. The experimental β_μ values for phosphine oxides **4** and **5** are more than 2 times greater than that of **1a** despite the fact that the intrinsic hyperpolarizabilities are smaller. Computational studies provide insight into the origin of the nonlinear optical response. The intrinsic hyperpolarizability of the monoaminophosphine oxide **1a** is comparable to that of 4-nitroaniline (**9**), while the onset of electronic absorption for **1a** occurs at *ca. 100 nm shorter wavelength* than **9**. Phosphine oxide **5** also has no onset of electronic absorptions greater than 300 nm. These observations have important ramifications in designing efficient materials with better transparency in the visible and near-UV spectral ranges.

Background

Because the nonlinear optical response in organic compounds is due to (hyper)polarization of the π electrons, the nonlinear response is of molecular origin. Consider the interaction of a single molecule with the strong electric field provided by intense laser light. The polarization, **P**, induced in the molecule by the external electric field, **E**, is typically expressed using one of the two following perturbation expansions:

$$\mathbf{P}_i = \alpha_{ij}\cdot\mathbf{E}_j + (1/2!)\beta_{ijk}\cdot\mathbf{E}_j\cdot\mathbf{E}_k + (1/3!)\gamma_{ijkl}\cdot\mathbf{E}_j\cdot\mathbf{E}_k\cdot\mathbf{E}_l + \ldots \quad (1)$$

$$\mathbf{P}_i = \alpha_{ij}\cdot\mathbf{E}_j + \beta_{ijk}\cdot\mathbf{E}_j\cdot\mathbf{E}_k + \gamma_{ijkl}\cdot\mathbf{E}_j\cdot\mathbf{E}_k\cdot\mathbf{E}_l + \ldots \quad (2)$$

where α_{ij} is the linear polarizability, β_{ijk} is the first hyperpolarizability, and γ_{ijkl} is the second hyperpolarizability.[8,9,38] The third-rank tensor β_{ijk}, which gives rise to second-order nonlinear optical phenomena (e.g., second-harmonic generation (SHG)), has properties similar to a vector and therefore vanishes in centrosymmetric molecules.[39] The fourth-rank tensor γ_{ijkl}, which gives rise to third-order nonlinear optical phenomena (e.g., third-harmonic generation (THG)), has the properties of a scalar and therefore is not subject to symmetry constraints. The terms higher than third order are often neglected and are not included in eqs 1 or 2.

The polarization induced in a bulk medium by an external electric field is given by a similar expression (for convenience, the tensorial nature of the coefficients is not expressed hereafter):

$$\mathbf{P} = \chi^{(1)}\cdot\mathbf{E} + \chi^{(2)}\cdot\mathbf{E}\cdot\mathbf{E} + \chi^{(3)}\cdot\mathbf{E}\cdot\mathbf{E}\cdot\mathbf{E} + \ldots \quad (3)$$

where $\chi^{(1)}$, $\chi^{(2)}$, and $\chi^{(3)}$ are the macroscopic susceptibilities related to the microscopic polarizabilities α, β, and γ. Like β, $\chi^{(2)}$ is subject to symmetry requirements and vanishes in centrosymmetric media. This represents an important consideration in designing or testing materials for second-order nonlinear optics: the bulk environment must be acentric in order to observe second-order nonlinear optical effects.

One unfortunate consequence of having two different conventions to express the induced polarization (eqs 1 and 2) is that the numerical values of the nonlinear coefficients are not directly comparable.[40] As defined in eqs 1 and 2, values of β differ by a factor of $^1/_2$, and values of γ differ by a factor of $^1/_6$. Additional numerical discrepancies may arise from improper treatment of degeneracy factors in different types of nonlinear optical processes.[40,41] Confusion frequently arises when comparing hyperpolarizabilities calculated using different computational methods and when comparing calculated values with experimental values, because the conventions used are not explicitly stated. For a detailed discussion of this issue, see ref 40.

Methodology

Semiempirical Computations. The geometry optimizations for **1**–**9** were performed at the AM1 level of theory[42] as implemented in the computational packages VAMP 5.0[43] and MOPAC 6.0.[44] For each molecule, the individual aryl rings were held planar to simplify the calculations. All other parameters were fully optimized using the keywords PERSIST and PRECISE. Semiempirical methods, and AM1 in particular, have proven to be adequate in predicting molecular structure of a variety of molecules, including molecules containing second-row elements such as sulfur.[21,27b,45] In addition, Dewar et al. demonstrated that their published AM1 parameters yield satisfactory results for both tricoordinate and tetracoordinate phosphorus.[46] Therefore, the AM1 method appears to be well-suited for computational studies of compounds **1**–**9**.[47,48] The calculations yield P=O bond lengths of 1.470–1.476 Å and O–P–C bond angles of 110.8–112.0° for compounds **1**–**6** (Table 1). The calculated values are in good agreement with experimental P=O bond lengths (1.470–1.512 Å) and O–P–C bond angles (110.2–112.9°) obtained from single-crystal X-ray analysis of several of the compounds.[49] In addition, calculated dipole moments of compounds **1**–**6** and **9** agree reasonably well with

(38) Shen, Y. R. *The Principles of Nonlinear Optics*; Wiley: New York, 1984.
(39) Levine, B. F.; Bethea, C. G. *J. Chem. Phys.* **1975**, *63*, 2666–2682.
(40) Willetts, A.; Rice, J. E.; Burland, D. M.; Shelton, D. P. *J. Chem. Phys.* **1992**, *97*, 7590–7599.
(41) Orr, B. J.; Ward, J. F. *Mol. Phys.* **1971**, *20*, 513–526.
(42) Dewar, M. J. S.; Zoebisch, E. G.; Healy, E. F.; Stewart, J. J. P. *J. Am. Chem. Soc.* **1985**, *107*, 3902–3909.
(43) Rauhut, G.; Alex, A.; Chandrasekhar, J.; Steinke, T.; Clark, T. Universität Erlangen–Nürnberg, 1993.
(44) Stewart, J. J. P. *Quantum Chemistry Program Exchange*; Indiana University, Bloomington, Indiana; Program 455, Version 6.0.
(45) Morley, J. O.; Docherty, V. J.; Pugh, D. *J. Chem. Soc., Perkin Trans. 2* **1987**, 1361–1363.
(46) Dewar, M. J. S.; Jie, C. *THEOCHEM* **1989**, *187*, 1–13.
(47) Given the limitations of our computing capabilities, computations involving ab initio methods with diffuse polarization functions and extensive configuration interaction are not feasible due to the size of the molecules being studied.
(48) For a detailed discussion of the bonding in phosphine oxides, see: Gilheany, D. G. *Chem. Rev.* **1994**, *94*, 1339–1374.
(49) (a) Kott, K. L.; Whitaker, C. M.; McMahon, R. J., manuscript submitted. (b) Kott, K. L. Ph.D. Dissertation, University of Wisconsin, Madison, WI, 1993.

Table 1. Calculated (AM1) P=O bond lengths and O–P–C Bond Angles for Phosphine Oxides 1–5

compound	P=O bond length[a]	O–P–C bond angles[b,c]
1a	1.475	111.0 ± 0.4
1b	1.474	111.0 ± 0.1
2a	1.476	110.9 ± 0.5
2b	1.474	110.9 ± 0.1
3a	1.476	110.9 ± 0.2
3b	1.475	110.9 ± 0.2
4	1.473	111.0 ± 1.5
5	1.470	112.0 ± 1.3

[a] In angstroms. [b] In degrees. [c] Calculated value represents an average over different low-energy conformations. The specified range does not define error limits (see text).

experimental values reported in this paper (Table 2). Hence, the AM1 method adequately reproduces experimental data for the compounds of interest.

The intrinsic hyperpolarizability $||\beta||$ is given by the magnitude of the vector component of the hyperpolarizability (β):[50]

$$||\beta|| = (\beta_x^2 + \beta_y^2 + \beta_z^2)^{1/2} \quad (4)$$

where β_x, β_y, and β_z are the vector components of the hyperpolarizability in the direction of the x, y, and z molecular axes, respectively. As we will see below, the VAMP and MOPAC programs use slightly different definitions of the vector components β_i.

The electric-field-induced second harmonic generation (EFISH) experiment does not measure the intrinsic hyperpolarizability, $||\beta||$; it measures the component of the hyperpolarizability in the direction of the dipole moment, β_μ. The quantity β_μ can also be obtained from the computed hyperpolarizability vector ($\boldsymbol{\beta}$) and dipole moment vector ($\boldsymbol{\mu}$) using the following relationships:

$$\cos\theta_{\beta\mu} = \frac{\boldsymbol{\mu}\cdot\boldsymbol{\beta}}{||\mu||\,||\beta||} \quad (5)$$

$$\beta_\mu = ||\beta||\cos\theta_{\beta\mu} = \frac{\boldsymbol{\mu}\cdot\boldsymbol{\beta}}{||\mu||} \quad (6)$$

where $\theta_{\beta\mu}$ is the angle between $\boldsymbol{\beta}$ and $\boldsymbol{\mu}$:

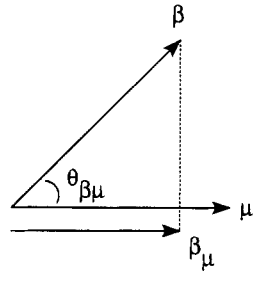

Sum-over-States Method. The ability to compute electronic excited states properly is a necessary prerequisite for computing hyperpolarizabilities by the sum-over-states method. Clark and Chandrasekhar demonstrated the ability of the AM1/CI method incorporated in VAMP 5.0[43] to compute the electronic spectra of

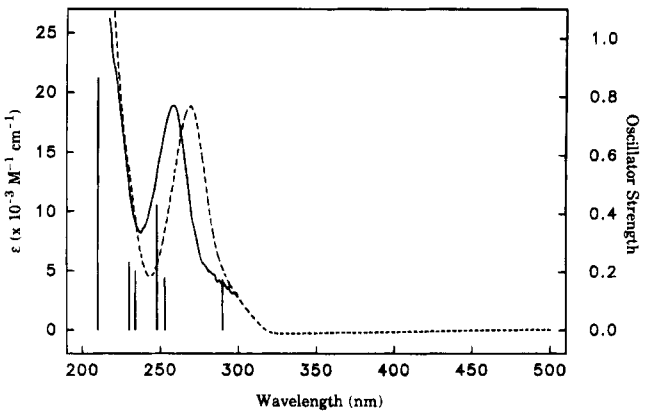

Figure 1. Experimental UV/vis spectra of (4-aminophenyl)-diphenylphosphine oxide (**1a**) in hexane (solid curve) and *p*-dioxane (dashed curve), plotted as molar extinction coefficient, ϵ, versus wavelength. (Note: saturated solution of **1a** in hexane is only ca. 10^{-5} M.) Calculated optical spectrum (bar plot) of **1a**, plotted as oscillator strength versus wavelength.

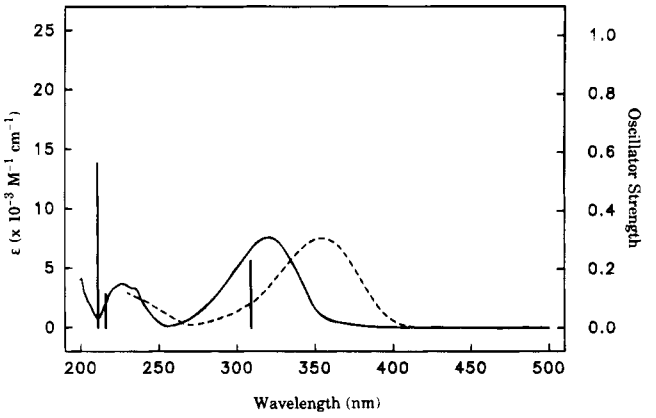

Figure 2. Experimental UV/vis spectra of 4-nitroaniline (**9**) in hexane (solid curve) and in *p*-dioxane (dashed curve), plotted as molar extinction coefficient, ϵ, versus wavelength. Calculated optical spectrum (bar plot) of **9**, plotted as oscillator strength versus wavelength.

organic molecules.[53] In the current study, the computed electronic spectra compare well with those measured experimentally, as demonstrated for compound **1a** in Figure 1 and for 4-nitroaniline (**9**) in Figure 2. This agreement gives us confidence that the VAMP calculations of hyperpolarizability permit meaningful comparisons of the compounds in Scheme 1, even if the absolute magnitudes of the hyperpolarizabilities involve some error.

First hyperpolarizabilities were calculated at 1064 nm by the sum-over-states method[51,52] following a configuration interaction (CI) including both single and pair-double excitations (PECI) using the VAMP 5.0 program.[53] The hyperpolarizability calculations for **1–9** utilized 12 active orbitals (PECI = 12) in the CI expansion, which included the 73 lowest-energy singlet excited states. For compounds **1–6**, the value of the hyperpolarizability converged satisfactorily when utiliz-

(50) The quantity $||\beta||$ is also commonly referred to as β_{vec}.

(51) (a) Morley, J. O.; Pavlides, P.; Pugh, D. *Int. J. Quantum Chem.* **1992**, *43*, 7–26. (b) Morley, J. O. *J. Am. Chem. Soc.* **1988**, *110*, 7660–7663. (c) Docherty, V. J.; Pugh, D.; Morley, J. O. *J. Chem. Soc., Faraday Trans.* **1985**, *81*, 1179–1192.

(52) Morrell, J. A.; Albrecht, A. C. *Chem. Phys. Lett.* **1979**, *64*, 46–50.

(53) (a) Clark, T.; Chandrasekhar, J. *Isr. J. Chem.* **1993**, *33*, 435–448. (b) Jain, M.; Chandrasekhar, J. *J. Phys. Chem.* **1993**, *97*, 4044–4049. (c) Rauhut, G.; Clark, T.; Steinke, T. *J. Am. Chem. Soc.* **1993**, *115*, 9174–9181.

ing 10 or more active orbitals in the CI expansion (51 excited states). For compounds **7**–**9**, the value of the hyperpolarizability converged satisfactorily when utilizing eight or more active orbitals in the CI expansion (33 excited states).

The VAMP program defines the vector components of the hyperpolarizability, $\beta_{i\text{VAMP}}$, in a manner consistent with the definitions utilized in most EFISH analyses:

$$\beta_{i\text{VAMP}} = {}^1/_2[{}^1/_3\sum_j(\beta_{ijj} + \beta_{jij} + \beta_{jji})] \quad (7)$$

For second-harmonic generation, the hyperpolarizability is invariant to permutation of the last two indices (i.e., $\beta_{ijk} = \beta_{ikj}$).[54] Equation 7 reduces to

$$\beta_{i\text{VAMP}} = {}^1/_2(\beta_{iii} + {}^1/_3\sum_{j\neq i}(\beta_{ijj} + 2\beta_{jji})) \quad (8)$$

where $i, j = x, y$, and z. One advantage of the sum-over-states method is that it explicitly treats the frequency dependence (dispersion) of the nonlinear coefficients. Kleinman symmetry does not apply under these circumstances.[55] The factor of $^1/_2$ in eqs 7 and 8 arises because of the differing conventions represented by eqs 1 and 2. The VAMP calculation corresponds to the convention used in eq 2.

Finite-Field Method. The MOPAC program defines the vector components of the hyperpolarizability, $\beta_{i\text{MOPAC}}$, as follows:[44,56]

$$\beta_{i\text{MOPAC}} = {}^1/_5\sum_j(\beta_{ijj} + \beta_{jij} + \beta_{jji}) \quad (9)$$

For second-harmonic generation, the hyperpolarizability is invariant to permutation of the last two indices (i.e., $\beta_{ijk} = \beta_{ikj}$).[54] Equation 9 reduces to

$$\beta_{i\text{MOPAC}} = {}^1/_5(3\beta_{iii} + \sum_{j\neq i}(\beta_{ijj} + 2\beta_{jji})) \quad (10)$$

Since the finite-field method in MOPAC 6.0 employs a static electric field, it cannot treat the frequency dependence of the nonlinear coefficients. In the absence of frequency dependence (dispersion), Kleinman symmetry applies.[55] The mathematical consequence of Kleinman symmetry is that the hyperpolarizability is invariant to permutation of all indices (i.e., $\beta_{ijj} = \beta_{jij} = \beta_{jji}$). Equation 10 further simplifies to

$$\beta_{i\text{MOPAC}} = {}^1/_5(3\beta_{iii} + \sum_{j\neq i}(3\beta_{ijj})) \quad (11)$$

$$= {}^1/_5(3\beta_{iii} + 3\beta_{ijj} + 3\beta_{ikk}) \quad (12)$$

$$= {}^3/_5(\beta_{iii} + \beta_{ijj} + \beta_{ikk}) \quad (13)$$

where $i, j, k = x, y, z$. The finite-field subroutine acknowledges the differing conventions represented by eqs 1 and 2 and therefore provides the computed values for the hyperpolarizability as β and $\beta/2$ and for the second hyperpolarizability as γ and $\gamma/6$. We report the larger value of β, which corresponds to the convention used in eq 1.

Electric-Field-Induced Second-Harmonic (EFISH) Generation. The EFISH experiment allows the determination of the component of the molecular hyperpolarizability along the direction of the molecular dipole moment, β_μ.[11a,39,57–61] The experiment thus provides accurate measurements of the hyperpolarizability, β_{ijk}, for molecules where the *dominant* component of the hyperpolarizability is along the direction of the dipole moment (e.g., $\beta_{ijk} \approx \beta_\mu$). This is often the case for molecules that are adequately described by the two-level model ($\beta_{CT} = \beta_\mu$).[8,9] However, the experiment does not provide an accurate measurement of the hyperpolarizability, β_{ijk}, if the dominant component of the hyperpolarizability is along a direction other than that of the dipole moment.

A complete treatment of the theory of electric-field-induced second-harmonic generation has been given by several authors.[11a,39,57–61] Essentially, the experimentally measured solution susceptibility is related to the molecular polarization by statistically averaging the contributions of the individual molecules. The macroscopic polarization of the solution at the second-harmonic frequency, $\mathbf{P}^{2\omega}$, produced by one static electric field and two optical fields at frequency ω, is given by

$$\mathbf{P}^{2\omega} = \Gamma\cdot\mathbf{E}^0\cdot\mathbf{E}^\omega\cdot\mathbf{E}^\omega \quad (14)$$

for all electric fields having a common polarization, where Γ is the bulk susceptibility of the solution. The term $\Gamma\cdot\mathbf{E}^0$ defines an effective second-order susceptibility, Γ_{eff}, so that the process resembles a second-order nonlinear optical effect:

$$\mathbf{P}^{2\omega} = \Gamma_{\text{eff}}\cdot\mathbf{E}^\omega\cdot\mathbf{E}^\omega \quad (15)$$

For a pure liquid, the third-order macroscopic (solution) susceptibility, Γ, is related to an effective microscopic (molecular) hyperpolarizability, γ^*, by

$$\Gamma = \text{N}[f]\gamma^* \quad (16)$$

where N is the number density of molecules, and $[f]$ is a product of local field factors defined by

$$[f] = f^0(f^\omega)^2(f^{2\omega}) \quad (17)$$

The local field factors compensate for the difference between the electric fields applied to the solution and the electric fields experienced by the molecule. We use local-field corrections described by Onsanger (vide infra).[59,62] There are two important contributions to γ^*:

(54) Reference 9, p 26.
(55) Kleinman symmetry implies no dispersion.[54]
(56) Kurtz, H. A.; Stewart, J. J. P.; Dieter, K. M. *J. Comput. Chem.* **1990**, *11*, 82–87.
(57) (a) Reference 8, pp 195–201. (b) Reference 9, pp 106–114.
(58) Bethea, C. G. *Appl. Opt.* **1975**, *14*, 1447–1451.
(59) (a) Teng, C. C.; Garito, A. F. *Phys. Rev. B* **1983**, *28*, 6766–6773. (b) Singer, K. D.; Garito, A. F. *J. Chem. Phys.* **1981**, *75*, 3572–3580.
(60) Oudar, J. L. *J. Chem. Phys.* **1977**, *67*, 446–457.
(61) (a) Burland, D. M.; Walsh, C. A.; Kajzar, F.; Sentein, C. *J. Opt. Soc. Am. B* **1991**, *8*, 2269–2281. (b) (c) Stähelin, M.; Moylan, C. R.; Burland, D. M.; Willetts, A.; Rice, J. E.; Shelton, D. P.; Donley, E. A. *J. Chem. Phys.* **1993**, *98*, 5595–5603.
(62) Onsager, L. *J. Am. Chem. Soc.* **1936**, *58*, 1486–1493:

$$f_i^0 = \epsilon_0\,(n_i^2 + 2)/(2\epsilon_0 + n_i^2)$$

$$f_i^\omega = f_i^{2\omega} = f_i^\infty = n_0^2(n_i^2 + 2)/(2n_0^2 + n_i^2)$$

$$\gamma^* = \gamma^e + \mu\cdot\beta_\mu/5kT \quad (18)$$

The first term, γ^e, is the purely electronic average third-order molecular hyperpolarizability and does not vanish for centrosymmetric molecules. The second term $\mu\cdot\beta_\mu/5kT$ is a temperature-dependent rotational term (where kT is the Boltzmann factor). It is proportional to the molecular ground-state dipole moment, μ, and the vector part of the second-order molecular hyperpolarizability in the direction of the molecular dipole moment, β_μ, which does vanish for centrosymmetric molecules. For a two component solution (L), a more general form of eq 16 results:

$$\Gamma_L = N_0[f_0]\gamma_0^* + N_1[f_1]\gamma_1^* \quad (19)$$

where the subscripts 0 and 1 refer to the solvent and solute molecules, respectively. Using Onsanger local field factors[59,62] and assuming that the refractive indices of the dilute solutions equal that of the pure solvent:

$$[f_0] = [f_1] = \epsilon_0(n_0^2 + 2)^4/27(2\epsilon_0 + n_0^2) \quad (20)$$

where ϵ_0 is the dielectric constant and n_0 is the refractive index of the pure solvent. Combining eqs 19 and 20

$$\Gamma_L = \frac{\epsilon_0(n_0^2 + 2)^4}{27(2\epsilon_0 + n_0^2)}[N_0\gamma_0^* + N_1\gamma_1^*] \quad (21)$$

By measuring Γ_L of a single solution and by known γ_0^* for the pure solvent, γ_1^* for the solute molecule of interest can be calculated using eq 21. Knowing γ_1^*, one can solve eq 11 for the product $\mu\cdot\beta_\mu$ by either measuring γ_1^e directly or assuming that $\mu\cdot\beta_\mu/5kT \gg \gamma_1^e$. Finally, independent measurement of μ (see below) permits calculation of β_μ. In this paper, we neglect contributions from γ_1^e. For some of the compounds in our study, this assumption may not be well-justified because β_μ values are small.

Alternatively, the infinite dilution extrapolation procedure of Singer and Garito[11a,59] allows a more accurate means of determining γ_1^*, and thus $\mu\cdot\beta_\mu$. The procedure involves measuring Γ_L, as well as the refractive index (n) and the dielectric constant (ϵ), at varying concentrations (10^{-2}–10^{-3} M) of solute. The slopes of y intercepts from the plots of each of the above physical properties versus weight fraction (w) of solute allows one to determine γ_1^* from

$$N_A\gamma_1^* = \frac{(2\epsilon_0 + n_1^2)(2n_0^2 + n_1^2)^3 MW_1}{(n_1^2 + 2)^4 n_0^6 \epsilon_0}\left[\frac{\partial\Gamma_L}{\partial w}v_0 + v_0\Gamma_0 - v_0\Gamma_0\left(\frac{1}{n_0^2}\frac{\partial n^2}{\partial w} + \left(\frac{1}{\epsilon_0} - \frac{2}{2\epsilon_0 + n_0^2}\right)\frac{\partial\epsilon}{\partial w}\right)\right] \quad (22)$$

where the factors Γ_0, ϵ_0, and n_0 are the y intercepts and the partial derivatives are the slopes of the corresponding plots, N_A is Avogadro's number, MW_1 is the molecular weight of the solute, and v_0 is the specific volume of the solvent. We assume that the refractive indices of the dilute solutions equal that of the pure solvent. The dielectric constant of each solution can be obtained by measuring the differential capacitance of the solution as described below.

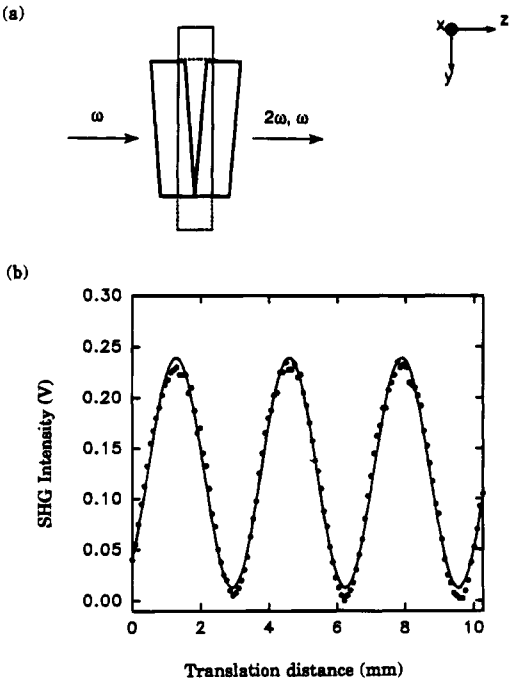

Figure 3. (a) Diagram of the EFISH solution cell (top view). (b) Maker fringe data for 4-nitroaniline (**9**) in *p*-dioxane.

The macroscopic solution susceptibility, Γ_L, is determined directly from the EFISH experiment.[11a,39,57–61] Briefly, a high-voltage pulse is applied to a solution of a dipolar NLO material contained in a wedge-shaped cell (Figure 3a). The molecular dipoles align along the direction of the electric field, thereby enabling the solution to exhibit second-harmonic generation. Translation of the wedge-shaped cell across the laser beam in the y direction produces a variation in path length which, in turn, generates a variation in the intensity of the second harmonic signal (Maker fringes, Figure 3b).[63,64] The Maker fringe data are analyzed via a least-squares fit to the following equation:[11a,59]

$$y = A_1\sin^2[(\pi/2)(l/A_3) + (A_4/2)] + A_2 \quad (23)$$

where $l = x\tan(\alpha)$, α being the wedge angle of the solution cell. In eq 23, $(A_1 + A_2)$ is the fringe maximum, A_2 is the fringe minimum, A_3 is the solution coherence length, l_c, and A_4 is the phase offset. From this least-squares fit, the mean intensity, $A_m = A_1/2 + A_2$, and coherence length, l_c, for the sample solution (L) and a reference solution (R) are used to calculate Γ_L from

$$\frac{A_m^L}{A_m^R} = \frac{E_0^L(T_1^L\Gamma_G l_c^G - T_2^L\Gamma_L l_c^L)^2[\exp(-2\alpha_\omega^L\bar{l}) + \exp(-\alpha_{2\omega}^L\bar{l})]}{E_0^R(T_1^R\Gamma_G l_c^G - T_2^R\Gamma_R l_c^R)^2[\exp(-2\alpha_\omega^R\bar{l}) + \exp(-\alpha_{2\omega}^R\bar{l})]} \quad (24)$$

where E_0 is the applied electric field, $\bar{l}$ is the mean value of the sample optical path length, α_ω and $\alpha_{2\omega}$ are the absorption coefficients at ω and 2ω, respectively, and

(63) Jerphagnon, J.; Kurtz, S. K. *J. Appl. Phys.* **1970**, *41*, 1667–1681.
(64) Maker, P. D.; Terhune, R. W.; Nisenoff, M.; Savage, C. M. *Phys. Rev. Lett.* **1962**, *8*, 21–22.

$$T_1 = t_{2\omega}{}^{G} t_{\omega}{}^{2}\{1/(n_{2\omega}{}^{G} + n_{\omega}{}^{G})\}\{(n_{\omega}{}^{G} + n_{2\omega}{}^{L})/(n_{2\omega}{}^{G} + n_{2\omega}{}^{L})\}$$

$$T_2 = t_{2\omega}{}^{G} t_{\omega}{}^{2} t^*{}_{\omega}{}^{2}\{1/(n_{2\omega}{}^{L} + n_{\omega}{}^{L})\}\{(n_{\omega}{}^{G} + n_{2\omega}{}^{L})/(n_{2\omega}{}^{G} + n_{2\omega}{}^{L})\}$$

where $t_{2\omega}{}^{G} = 2n_{2\omega}{}^{G}/(1 + n_{2\omega}{}^{G})$, $t_{\omega} = 2/(1 + n_{\omega}{}^{G})$, and $t^*{}_{\omega} = 2n_{\omega}{}^{G}/(n_{\omega}{}^{G} + n_{\omega}{}^{L})$. The superscripts G and L refer to the glass windows and the liquid sample. As described previously, measurement of Γ_L permits evaluation of $\gamma_1{}^*$ using either eq 21 or eq 22, and hence $\mu\cdot\beta_\mu$ using eq 18. Independent measurement of μ (see below) permits calculation of β_μ.

All of the nonlinear susceptibilities expressed in eq 24 are referenced, directly or indirectly, to the susceptibility of quartz.[40] The susceptibility of quartz is, in turn, directly referenced to the absolute susceptibility of $LiIO_3$.[65] Unfortunately, the literature values for d_{31} ($LiIO_3$) differ by 40%.[66] In our analyses, we used literature values for Γ_G (BK-7 glass) = 3.5×10^{-14} esu[59] and Γ_L (*p*-dioxane) = 5.2×10^{-14} esu[59a,61] that were measured relative to the earlier value of d_{31} ($LiIO_3$),[66a] which corresponds to $\chi^{(2)}{}_{111}$ (quartz) = $2d_{11}$ (quartz) = 2.4×10^{-9} esu.[65] A table containing all of the numerical constants used in the analysis of the EFISH experiment is available as supplementary material.

Dielectric Constants and Dipole Moments. Since the EFISH experiment gives $\mu\cdot\beta_\mu$, it is necessary to determine the ground-state dipole moment, μ, separately. Ground-state dipole moments are determined from an analysis of the solution dielectric constant versus concentration (10^{-2}–10^{-3} M) of solute, using *p*-dioxane as the solvent.[67–70] The dielectric constant of each solution is determined by measuring the differential capacitance of the solution. Capacitance measurements are made utilizing a Stanford Research Systems Model SR270 LCR meter, using a two-terminal stainless steel electrode cell.[71] Measurement of the capacitance of air (empty cell), C_a, and of pure solvent, C_0, allows calculation of the cell constant, C_c, and the ground capacitance, C_g, of the cell from

$$C_c = (C_0 - C_a)/(\epsilon_0 - \epsilon_a) \quad (25)$$

$$C_g = C_a - C_c \quad (26)$$

where $\epsilon_a = 1.000$ is the dielectric constant of air, and ϵ_0 is the dielectric constant of pure solvent ($\epsilon_0 = 2.209$ for *p*-dioxane).[72] The dielectric constant of a solution containing solute, ϵ_1, is then given by

$$\epsilon_1 = (C_s - C_g)/C_c \quad (27)$$

where C_s is the measured capacitance of the solution. To calculate the ground-state dipole moment, the dielectric constant of the solution is related to the molar polarization of the solute, P_1:

$$(P_1 - P_0)[C] + P_0/V = \{(\epsilon_1 - 1)(\epsilon_1 + 2)/8\epsilon_1\} - \{(n_1{}^2 - 1)(n_1{}^2 + 2)/8n_1{}^2\} \quad (28)$$

where [C], V, and n_1 refer to the concentration (mol/cm^3), molar volume, and refractive index of the solution, and $P_0 = MW_0/d_0 \times (\epsilon_0 - 1)/(\epsilon_0 + 2)$ is the molar polarization of the solvent; MW_0, d_0, and ϵ_0 refer to the molecular weight, density, and dielectric constant of the pure solvent, respectively. Assuming that the refractive indices of the dilute solutions are equal to that of the pure solvent, eq 28 becomes

$$\{(\epsilon_1 - 1)(\epsilon_1 + 2)/8\epsilon_1\} = (P_1 - P_0)[C] + P_0/V + \{(n_0{}^2 - 1)(n_0{}^2 + 2)/8n_0{}^2\} \quad (29)$$

Plotting $\{(\epsilon_1 - 1)(\epsilon_1 + 2)/8\epsilon_1\}$ versus [C] yields a slope of $(P_1 - P_0)$ and a y intercept of $P_0/V + \{(n_0{}^2 - 1)(n_0{}^2 + 2)/8n_0{}^2\}$. The ground-state dipole moment, μ, is related to the molar polarization of the solute, P_1, obtained from the slope of the plot, by

$$P_1 = (4\pi N_A \mu^2)/9kT \quad (30)$$

where N_A is Avogadro's number, k is the Boltzmann constant, and T is the temperature in kelvin.

Powder Second-Harmonic Generation (Powder SHG). Powder SHG experiments[73] provide a relatively quick and easy means of screening compounds in the solid state for second-order nonlinear optical response. Only compounds that exist in a noncentrosymmetric environment in the solid state are capable of SHG; the experiment thus immediately identifies compounds that crystallize in noncentrosymmetric space groups. Because the intensity of the observed second-harmonic signal generated by the powdered sample depends on the particle size,[3,73] the experiment provides at best only a semiquantitative measure of $\chi^{(2)}$, and comparison of the results must be made with care. The experiment utilizes a Continuum model NY-61 Q-switched Nd:YAG laser operating at a fundamental wavelength of 1064 nm (10 Hz repetition rate, 6 ns pulse width). The laser beam is attenuated and vertically (s) polarized as described in the experimental section. An unfocused beam of about 1.0 mJ average power is passed through a thin layer of a finely powdered sample of the compound placed between two ordinary glass microscope slides. After filtering out the transmitted 1064 nm light, the transmitted second harmonic at 532 nm is detected by means of a photomultiplier tube. The second-harmonic intensity of the sample is reported relative to the second-harmonic intensity from a finely powdered sample of urea.[74]

Results

Semiempirical Computations. Table 2 contains the calculated values of the magnitude of the first

(65) Jerphagnon, J. *Appl. Phys. Lett.* **1970**, *16*, 298–299. See also: Meredith, G. R. *Phys. Rev. B* **1981**, *24*, 5522–5532.
(66) (a) Choy, M. M.; Byer, R. L. *Phys. Rev. B* **1976**, *14*, 1693–1706. (b) Eckardt, R. C.; Masuda, H.; Fan, Y. X.; Byer, R. L. *IEEE J. Quantum Electron.* **1990**, *26*, 922–933.
(67) Thami, T.; Bassoul, P.; Petit, M. A.; Simon, J.; Fort, A.; Barzoukas, M.; Villaeys, A. *J. Am. Chem. Soc.* **1992**, *114*, 915–921.
(68) Exner, O. *Dipole Moments in Organic Chemistry*; Georg Thieme Publishers: Stuttgart, 1975.
(69) Minkin, V. I.; Osipov, O. A.; Zhdanov, Y. A. *Dipole Moments in Organic Chemistry*; Plenum Press: New York, 1970.
(70) Guggenheim, E. A. *Trans. Faraday Soc.* **1949**, *45*, 714–720.
(71) For a detailed description of the capacitance cell, see: Kott, K. L. Ph.D. Dissertation, University of Wisconsin–Madison, 1993.
(72) *CRC Handbook of Chemistry and Physics*; CRC Press: Boca Racon, FL, 1985.
(73) Kurtz, S. K.; Perry, T. T. *J. Appl. Phys.* **1968**, *39*, 3798–3813.
(74) Francis, C. V.; Tiers, G. V. D. *Chem. Mater.* **1992**, *4*, 353–358.

Table 2. Calculated and Experimental Hyperpolarizability and Dipole Moment Data for 1–9

cmpd	$\mu^{a,b,c}$ calc	$\mu^{c,d}$ expt	$\|\beta\|^{a,e,f}$ MOPAC	$\beta_\mu{}^{a,e,f}$ MOPAC	$\theta_{\beta\mu}{}^{a,g}$ MOPAC (deg)	$\|\beta\|^{e,f,h}$ VAMP	$\beta_\mu{}^{a,f,h}$ VAMP	$\theta_{\beta\mu}{}^{a,g}$ VAMP (deg)	$\beta_\mu{}^{f,i}$ expt	$\lambda_{max}{}^{d,l}$
1a	6.2 ± 0.4	5.5	3.6 ± 0.1	1.2 ± 0.2	71 ± 4	28.7 ± 1.1	2.0 ± 1.3	88 ± 4	4.3	264
2a	6.4 ± 0.7		3.8 ± 0.5	2.3 ± 0.8	50 ± 19	16.3 ± 2.7	3.2 ± 3.1	80 ± 11	4.0	266
3a	6.9 ± 1.5		2.9 ± 0.5	2.7 ± 0.5	15 ± 15	9.0 ± 4.1	3.4 ± 4.0	68 ± 34		
1b	5.2 ± 1.0	7.6	1.7 ± 0.1	−0.6 ± 0.3	109 ± 8	11.6 ± 4.9	−7.3 ± 2.6	131 ± 4	4.6[j]	238
2b	4.5 ± 1.3	5.9	1.6 ± 0.1	0.4 ± 0.2	82 ± 15	9.1 ± 4.8	−7.2 ± 4.4	145 ± 16	1.5	240
3b	5.0 ± 3.0	5.7	0.8 ± 0.4	0.7 ± 0.5	14 ± 14	6.9 ± 4.4	−4.0 ± 3.0	126 ± 9	1.0	242
4	8.1 ± 0.4	8.3	4.2 ± 0.2	2.9 ± 0.2	46 ± 3	19.7 ± 4.8	11.2 ± 3.6	56 ± 3	9.0[k]	340
5	7.0 ± 0.1	4.7	3.9 ± 0.1	3.4 ± 0.1	28 ± 3	17.0 ± 0.0	13.5 ± 2.1	36 ± 12	10.1[k]	298
6	5.3	4.8	1.2	−1.2	180	6.2	−6.0	165	<0.8	272
7	6.5 ± 0.3		3.0	1.4	61	22.4 ± 0.6	8.9 ± 2.4	67		
8	7.2		1.8	1.3	44	4.1	3.3	36		
9	7.3	7.4	5.5	5.4	10	16.9	16.6	11	19.2	355

[a] Calculated value represents an average over different low-energy conformations. The specified range does not define error limits (see text). [b] Both MOPAC and VAMP provide the same computed value of the dipole moment. [c] In units of debye. [d] In *p*-dioxane. [e] Static hyperpolarizability computed using the AM1/finite-field method. [f] In units of 10^{-30} cm^5 esu^{-1}. [g] Computed from the calculated components of μ and β using eq 5. [h] Hyperpolarizability computed using the AM1/sum-over-states method at 1064 nm. [i] EFISH measurement in *p*-dioxane at 1064 nm. [j] In $CHCl_3$. [k] Determined using the infinite dilution method. [l] In units of nanometers.

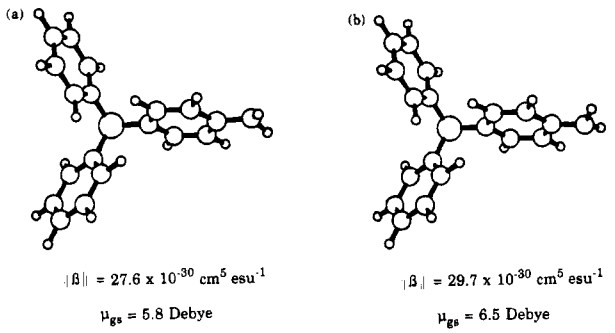

Figure 4. Two optimized, minimum energy conformations for (4-aminophenyl)diphenylphosphine oxide (**1a**), as viewed down the phosphorus–oxygen bond (oxygen atom in back). Structure (b) differs from (a) only by a 180° rotation (inversion) of the *p*-amino substituent.

molecular hyperpolarizability, $\|\beta\|$, the ground-state dipole moment, μ, the component of the hyperpolarizability in the direction of the dipole moment, β_μ, and the angle between the hyperpolarizability and dipole moment vectors, $\theta_{\beta\mu}$, for phosphine oxides **1–8** and 4-nitroaniline (**9**). The sum-over-states (VAMP) calculation of β_μ for 4-nitroaniline (**9**, 16.6×10^{-30} cm^5 esu^{-1}) is an excellent agreement with previously reported experimental values (16.9×10^{-30} cm^5 esu^{-1}).[59a]

The AM1-optimized geometry for compounds **1–4** is a propellar arrangement of the three aryl rings about the central phosphorus–oxygen (P=O) bond. In each compound, the dihedral angle between the plane of any one of the aryl rings and the corresponding plane defined by C_{ipso}, P, and O is ca. 26–27°. In this propeller arrangement, the two faces of each of the aryl rings are nonequivalent. Since each amino substituent is pyramidal, it may achieve one of two nonequivalent orientations. For compound **1a**, the two minima differ only by a 180° rotation (or inversion) of the amino group (Figure 4). In Figure 4a, the nitrogen lone pair lies on the same face of the aryl ring as the P=O bond, whereas in Figure 4b the nitrogen lone pair lies on the opposite face. Optimization of various starting geometries invariably leads to one of these two minimized structures; no other minima were obtained. Not surprisingly, the conformation of the para substituents affects the calculated values of $\|\beta\|$ and μ. We probed this effect in detail using the sum-over-states (VAMP) calculations. For **1a**, the hyperpolarizability ($\|\beta\| = 27.6 \times 10^{-30}$ cm^5 esu^{-1}, 29.7×10^{-30} cm^5 esu^{-1}) and the ground-state dipole moment ($\mu = 5.8$, 6.5 D) both change upon rotation of the amino group. The monosubstituted compounds (**1**) show two low-energy conformations, and the disubstituted and trisubstituted compounds (**2** and **3**) show four low-energy conformations. We obtained energy minima for all possible combinations of 180° rotations of the para amino and hydroxy substituents. The $\|\beta\|$, μ, β_μ, and $\theta_{\beta\mu}$ values reported in Table 2 are the average of the values obtained from the individual conformations with the smallest and largest values of $\|\beta\|$, μ, β_μ, and $\theta_{\beta\mu}$. The ranges given in Table 2 represent the difference of the average values from these extremes. These ranges do not represent error limits.

The hyperpolarizability $\|\beta\|$ depends slightly on the distortion of the aryl rings from planarity, but we found this effect to be minor. We therefore simplified the calculations by holding all of the aryl rings planar.

The magnitude of $\|\beta\|$ is very sensitive to molecular conformation. Rotation of the aryl rings about the phosphorus–carbon bonds dramatically changes $\|\beta\|$. We investigated this conformational dependence of $\|\beta\|$ in detail using sum-over-states (VAMP) calculations of the model diaryl phosphine oxide **7** (Scheme 1). In the AM1-optimized geometry for **7**, the plane defined by aryl ring (a) (see Figure 5) is nearly parallel to the corresponding plane defined by C_{ipso}, P, and O; the dihedral angle θ between the two planes is 5°. The dihedral angle ϕ between the plane of aryl ring (b) and the corresponding plane defined by C'_{ipso}, P, and O is 30°. To isolate the effect on $\|\beta\|$ of the conformational rotation of the aryl rings, the dihedral angle θ was held at 5° (aryl ring (a) fixed), and dihedral angle ϕ was rotated from 0° to 90° in 10° increments (aryl ring (b) rotated). At each increment, the remaining parameters were reoptimized, and $\|\beta\|$ recalculated. This rotation produces a significant effect on the magnitude of the hyperpolarizability, $\|\beta\|$; $\|\beta\|$ decreases dramatically upon rotation of aryl ring (b) from a coplanar to a perpendicular conformation with respect to the P=O bond (Figure 5).[75] Such a result can be explained in terms of decreased orbital overlap of the π-electron system of aryl ring (b) with the P=O moiety, and, more importantly, with the π-electron system of aryl ring (a). This latter point is further demonstrated by comparing the calculated value of $\|\beta\|$ of diarylphos-

(75) A similar conformational dependence of $\|\beta\|$ was observed for the rotation of dihedral angle θ from 0° to 90° (aryl ring (a) rotated) while holding dihedral angle ϕ at 30° (aryl ring (b) fixed).

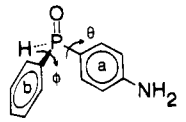

7

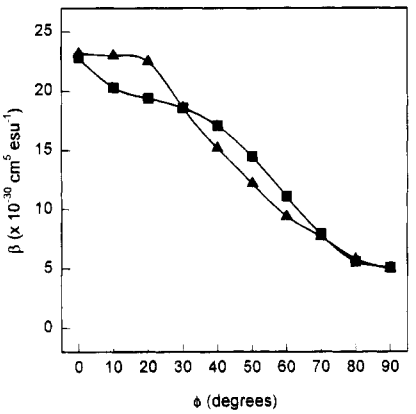

Figure 5. (■) Conformational dependence of $||\beta||$ on the rotation of aryl ring (b), with aryl ring (a) fixed at a dihedral angle of 5°, for **7**. The data are plotted as $||\beta||$ versus the dihedral angle, ϕ, between the plane of aryl ring (b) and the phosphorus-oxygen bond. (▲) Conformational dependence of $||\beta||$ on the rotation of aryl ring (b), allowing aryl ring (a) to reoptimize at each increment, for **7**. The data are plotted as $||\beta||$ versus the dihedral angle, ϕ, between the plane of aryl ring (b) and the phosphorus−oxygen bond.

phine oxide **7** (22.4×10^{-30} cm^5 esu^{-1}) with that of monoarylphosphine oxide **8** (4.1×10^{-30} cm^5 esu^{-1}); $||\beta||$ is much larger for **7** than for **8**. The presence of the second aryl ring (b) *in conjugation with* the first aryl ring (a) is clearly a requirement to achieve a large hyperpolarizability. The calculated barrier to rotation of the phenyl rings is 3−5 kcal/mol.

In a related conformational study, dihedral angle ϕ in **7** was again rotated from 0° to 90° in 10° increments, but instead of holding aryl ring (a) in a fixed position, it was allowed to reoptimize at each increment.[76] The overall dependence of $||\beta||$ on ϕ (Figure 5) is similar to that obtained when aryl ring (a) was held in a fixed position (Figure 5).

Previous theoretical studies report a similar conformational dependence of the hyperpolarizability upon rotation of aryl rings in donor−acceptor substituted stilbenes,[20] diaryl acetylenes,[30] bi- and polyphenyls,[19] and 2-methylene-4-phenyl-1,3-dithioles.[77] In addition, a conformational dependence of the hyperpolarizability has been observed upon rotation of the donor and acceptor substituents in 4-nitroaniline, aniline, and nitrobenzene,[78] as well as in 4-(dimethylamino)benzonitrile[79,80] and 4-(dimethylamino)nitrosobenzene.[80]

Nonlinear Optical Measurements. Table 2 contains the experimental values of the ground-state dipole moment, μ, and the component of the hyperpolarizability in the direction of the dipole moment, β_μ, for compounds **1**−**6** and 4-nitroaniline (**9**). The β_μ value measured for 4-nitroaniline (**9**, 19.2×10^{-30} cm^5 esu^{-1}) agrees reasonably well with previously reported EFISH measurements (16.9×10^{-30} cm^5 esu^{-1}).[59a] Because of the small β_μ values for compounds **1**−**3** and **6**, only solutions near the saturation limit for these materials (ca. 10^{-2} M) produced second-harmonic signals that differed significantly from that of the pure solvent. Thus, a concentration dependence could not be performed for these compounds, and $\mu\cdot\beta_\mu$ was measured for individual solutions. The di- and trisubstituted compounds **4** and **5** did not suffer from either poor solubility or a small β_μ; therefore, concentration-dependent analyses of the molecular hyperpolarizabilities were performed. Because the electronic absorptions of phosphine oxides **1**−**3** and **6** occur at less than 280 nm, correcting for resonance effects has little effect on β_μ values.[25a,81,82]

Table 3. Powder SHG and X-ray Crystallography Data for 1−5

compound	$I_{2\omega}$[a]	symmetry	crystal space group
1a	0.01	noncentrosymmetric	*Cc*, monoclinic
1b	1	noncentrosymmetric	$Pca2_1$, orthorhombic
2a	0	centrosymmetric	
2b	0	centrosymmetric	$P2_1/c$, monoclinic
3b	0	centrosymmetric	$P2_1/c$ monoclinic
4	1	noncentrosymmetric	
5	0	centrosymmetric	

[a] Relative to urea.

Table 3 contains powder SHG and X-ray crystallography data for compounds **1**−**5**.[83] The detailed X-ray crystal structure data for phosphine oxides **1a**, **1b**, **2b**, and **3b** are discussed in detail elsewhere.[49] All powder SHG experiments were performed at a fundamental wavelength of 1064 nm, and are reported as $I_{2\omega}$ relative to urea.

Discussion

The computational results obtained from the MOPAC (AM1/finite field) and VAMP (AM1/sum-over-states) computations exhibit qualitative agreement concerning certain aspects of the nonlinear optical response of substituted arylphosphine oxides. Both methods implicate charge transfer from a donor-substituted aryl ring to either an acceptor-substituted aryl ring or an

(76) A similar conformational dependence of $||\beta||$ was observed for the rotational of dihedral angle θ from 0° to 90° (aryl ring (a) rotated), allowing dihedral angle ϕ to reoptimize at each 10° increment.

(77) Kodaka, M.; Fukaya, T.; Yonemoto, K.; Shibuya, I. *J. Chem. Soc., Chem. Commun.* **1990**, 1096−1098.

(78) Velders, G. J. M.; Gillet, J.-M.; Becker, P. J.; Feil, D. *J. Phys. Chem.* **1991**, *95*, 8601−8608.

(79) Leung, P. C.; Stevens, J.; Harelstad, R. E.; Spiering, M. S.; Gerbi, D. J.; Francis, C. V.; Trend, J. E.; Tiers, G. V. D.; Boyd, G. T.; Ender, D. A.; Williams, R. C. *Proc. SPIE* **1989**, *1147*, 48−60.

(80) Sen, R.; Majumdar, D.; Bhattacharyya, S. P.; Bhattacharyya, S. N. *Chem. Phys. Lett.* **1991**, *181*, 288−292.

(81) According to the two-level model, the relationship between β_0 and β_ω is given by

$$\beta_0 = \beta_\omega\{(\omega_0^2 - 4\omega^2)(\omega_0^2 - \omega^2)\}/\omega_0^4$$

where ω is the fundamental laser frequency, ω_0 is the frequency of the electronic transition, β_0 is the hyperpolarizability at zero frequency, and β_ω is the hyperpolarizability at frequency ω.[25a]

(82) When corrected for dispersion using the two-level model, the static hyperpolarizability β_0 differs little from β_μ. The AM1/sum-over-states computations indicate that several excited states contribute appreciably to the first hyperpolarizability (vide infra), and thus the two-level model would not apply to compounds **1**−**5**.

(83) Compound **1a** crystallizes as colorless prisms in the monoclinic space group *Cc*: a = 17.462(3) Å, b = 17.557(4) Å, c = 21.301(4) Å, β = 98.40(3)°, and Z = 16. Compound **1b** crystallizes as colorless prisms in the orthorhombic space group $Pca2_1$: a = 18.092(9) Å, b = 10.325(5) Å, c = 16.292(3) Å, and Z = 8. Compound **2b** crystallizes as colorless prisms in the monoclinic space group $P2_1/c$: a = 8.9406(1) Å, b = 15.101(3) Å, c = 15.954(3) Å, β = 101.14(2)°, and Z = 4. Compound **3b** crystallizes as colorless prisms in the monoclinic space group $P2_1/c$: a = 9.225(3) Å, b = 15.033(4) Å, c = 15.874(5) Å, β = 102.59(3)°, and Z = 4.

unsubstituted phenyl ring as the major contributor to molecular hyperpolarizability. This result is revealed directly in the VAMP (sum-over-states) calculation by analysis of the excited-state contributions to β and is revealed indirectly in the MOPAC (finite field) calculation by the large value of $\theta_{\beta\mu}$ (vide infra). In contrast to our initial expectations, the phosphoryl substituent (P=O) does not serve as the electron acceptor in the charge-transfer excited states. For any given series of compounds, the two computational methods offer somewhat different predictions for the values of both $||\beta||$ and $\theta_{\beta\mu}$. As a consequence, the methods yield different trends in the calculated values of β_μ. Neither method reliably predicts all of the trends observed in the experimental values of β_μ.

Both MOPAC (AM1/finite field) and VAMP (AM1/sum-over-states) calculations reveal that phosphine oxides **1**–**6** possess moderate intrinsic molecular hyperpolarizabilities $||\beta||$ (Table 2). For phosphine oxides **1a**, **2a**, **4**, and **5**, MOPAC predicts $||\beta||$ values that are 65–76% of the value for 4-nitroaniline (**9**), while VAMP predicts $||\beta||$ values that are 95–170% of the value for 4-nitroaniline (**9**). It is surprising and important that these phosphine oxides, with a weaker electron acceptor and minimal charge transfer from the electron-donating substituent to the phosphine oxide acceptor, are calculated to possess hyperpolarizabilities comparable to 4-nitroaniline (**9**). Comparison of the amino-substituted phosphine oxides with the hydroxy-substituted phosphine oxides reveals that the amino-substituted phosphine oxides possess larger $||\beta||$. Thus, for the arylphosphine oxides, the combination of NH_2/P=O leads to a larger intrinsic hyperpolarizability than the combination of OH/P=O. This is consistent with previous theoretical[25a] and experimental[12a] observations that nitroanilines possess larger molecular hyperpolarizabilities than nitrophenols.

Most surprising to us, both MOPAC and VAMP predict that the direction of largest hyperpolarizability in 4-(aminophenyl)diphenylphosphine oxide (**1a**) lies nearly orthogonal to the direction of the P–O bond, as evidenced by the large computed values of $\theta_{\beta\mu}$ (Table 2). This suggests that the two unsubstituted phenyl rings, not the phosphoryl group (P=O), serve as the electron acceptor. To further investigate this possibility, we performed computational studies (VAMP) on model phosphine oxides **7** and **8**, which lack one or both of the unsubstituted phenyl rings. The computational studies of **7** and **8** reveal a substantial increase in $||\beta||$ for diarylphosphine oxide **7** compared to monoarylphosphine oxide **8**. In fact, the small $||\beta||$ value for **8** indicates that the H_2P=O group alone is a poor acceptor for NLO materials. However, substitution of the P=O group with an additional phenyl group, as in **7**, leads to a significant enhancement of the hyperpolarizability, $||\beta||$. Molecular orbital (MO) analyses of **7** and **8** provide an understanding of the role of the additional phenyl ring in enhancing the hyperpolarizability of **7**. Figure 6 shows the MO diagram for diarylphosphine oxide **7**, obtained from the AM1/sum-over-states computations,[84] and Table 4 lists selected excited states which may

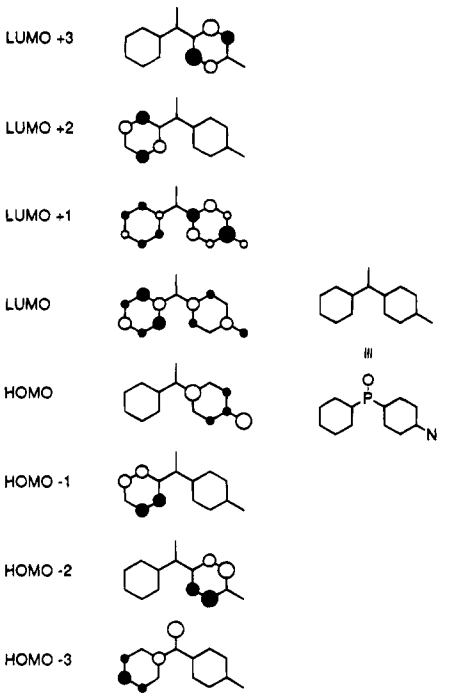

Figure 6. Molecular orbital diagram for diarylphosphine oxide **7**.

Table 4. Change in Dipole Moment, $\Delta\mu$, Oscillator Strength, and Energy for the Excited States Which May Contribute to $||\beta||$ for Diarylphosphine Oxide 7

excited state[a]	$\Delta\mu$ (D)	oscillator strength	energy eV	energy nm	major transitions (weight)
10 (S_2)	15.10	0.182	4.33	286.3	HOMO → LUMO (0.31)
					HOMO → LUMO +1 (0.52)
					HOMO −2 → LUMO +3 (0.31)
16 (S_6)	9.11	0.399	6.01	206.3	HOMO → LUMO +3 (0.40)
					HOMO → LUMO +4 (0.23)
					HOMO −2 → LUMO (0.24)
					HOMO −2 → LUMO +1 (0.40)
26 (S_{12})	9.19	1.062	6.66	186.3	HOMO −1 → LUMO (0.33)
					HOMO −1 → LUMO +1 (0.19)
					HOMO −3 → LUMO +2 (0.31)
					HOMO −4 → LUMO +2 (0.28)
					HOMO −5 → LUMO +2 (0.25)
28 (S_{13})	8.09	0.427	6.76	183.4	HOMO −1 → LUMO +2 (0.21)
					HOMO −2 → LUMO +3 (0.13)
					HOMO −3 → LUMO +1 (0.47)
					HOMO −5 → LUMO (0.20)
					HOMO −5 → LUMO +1 (0.29)
29 (S_{14})	5.99	0.469	6.88	180.1	HOMO −1 → LUMO +2 (0.33)
					HOMO −2 → LUMO +3 (0.23)
					HOMO −3 → LUMO (0.24)
					HOMO −5 → LUMO (0.21)
					HOMO −5 → LUMO +1 (0.30)

[a] The excited states correspond exactly as listed in the AM1/sum-over-states output.

contribute to $||\beta||$.[85] Table 4 indicates that several excited states could contribute significantly to $||\beta||$; therefore, the arylphosphine oxides are not adequately described by the two-level model. Inspection of the these excited states reveals that several of the transitions involve transfer of charge from the amino donor and the amino-substituted aryl ring to the unsubstituted aryl ring; these transitions include: highest occupied molecular orbital (HOMO) → lowest unoc-

(84) Hyperpolarizability $||\beta||$ was computed using 12 active orbitals (PECI = 12). For compounds **7** and **8**, our results establish that $||\beta||$ converges satisfactorily when utilizing eight or more active orbitals. For simplicity, only 8 of the 12 active orbitals are shown in the molecular orbital analyses depicted in Figure 6 and Table 4.

(85) The excited states listed in Tables 4 and 5 were selected from the list of all computed singlet states because they have a large change in dipole moment and/or a high oscillator strength.

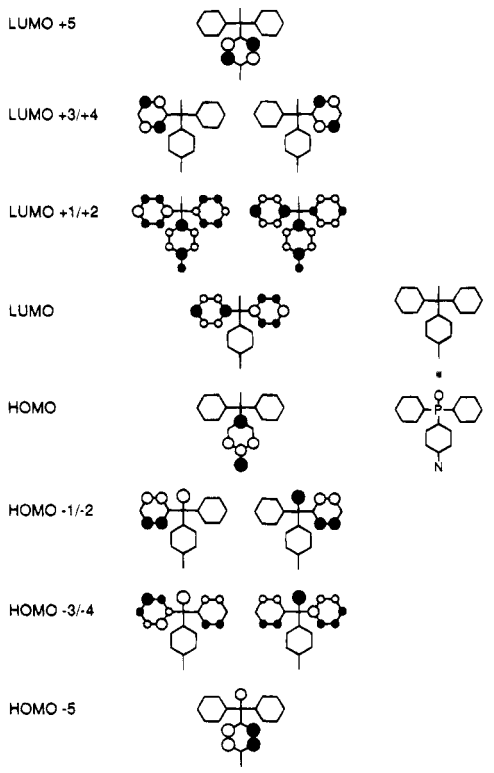

Figure 7. Molecular orbital diagram for (4-aminophenyl)-diphenylphosphine oxide (**1a**).

cupied molecular orbital (LUMO), HOMO → LUMO +1, HOMO → LUMO +3, HOMO −2 → LUMO, and HOMO −2 → LUMO +1. Three of the transitions, HOMO −1 → LUMO, HOMO −1 → LUMO +1, and HOMO −2 → LUMO +3, involve transfer of charge from the unsubstituted aryl ring to the amino-substituted aryl ring. Significantly, none of the transitions involve charge transfer from the amino donor to the phosphoryl moiety. For monoarylphosphine oxide **8**, the transitions contributing to $||\beta||$ involve transfer of charge from the amino donor to the aryl ring and from the phosphoryl oxygen to the aryl ring. Again, none of the transitions involve charge transfer from the amino donor to the phosphoryl moiety. Upon comparison of **7** and **8**, we conclude that achieving large $||\beta||$ for the arylphosphine oxides requires substantial overlap of at least two aryl rings, one of which bears the electron-donor substituent. The strongly donating amino (or hydroxy) group serves to additionally polarize the π-electron system. Thus, the hyperpolarizability of these molecules arises from movement of the π-electron density from one aryl ring through the P=O group to the other aryl ring(s) *without* a significant degree of electron transfer from the amino-donor substituent to the P=O acceptor substituent.[86]

The MO analysis of (aminophenyl)diphenylphosphine oxide (**1a**) again reflects the importance of the unsubstituted aryl rings. Figure 7 shows the MO diagram for **1a**,[87] and Table 5 lists the excited states which may contribute to $||\beta||$.[85] The MO diagram for the monohydroxy phosphine oxide **1b** is analogous to that for **1a**.

Table 5. Change in Dipole Moment, $\Delta\mu$, Oscillator Strength, and Energy for the Excited States Which May Contribute to $||\beta||$ for (4-Aminophenyl)diphenylphosphine Oxide (1a)

excited state[a]	$\Delta\mu$ (D)	oscillator strength	energy eV	energy nm	major transitions (weight)
11 (S_2)	15.85	0.175	4.28	289.7	HOMO → LUMO +1 (0.40)
					HOMO → LUMO +2 (0.46)
					HOMO −5 → LUMO +5 (0.31)
13 (S_4)	7.66	0.417	5.01	247.6	HOMO −1 → LUMO (0.38)
					HOMO −1 → LUMO +1 (0.20)
					HOMO −2 → LUMO +1 (0.26)
					HOMO −2 → LUMO +2 (0.22)
					HOMO −3 → LUMO +1 (0.18)
					HOMO −4 → LUMO (0.22)
18 (S_7)	4.98	0.888	5.94	208.8	HOMO → LUMO +5 (0.32)
					HOMO −3 → LUMO +2 (0.17)
					HOMO −4 → LUMO (0.22)
					HOMO −5 → LUMO +1 (0.28)
					HOMO −5 → LUMO +2 (0.25)
					HOMO −5 → LUMO +5 (0.25)
19 (S_8)	3.74	0.673	5.97	207.5	HOMO → LUMO +5 (0.29)
					HOMO −4 → LUMO (0.20)
					HOMO −5 → LUMO +1 (0.19)
					HOMO −5 → LUMO +2 (0.23)
					HOMO −5 → LUMO +5 (0.33)
20 (S_9)	4.36	0.341	6.06	204.6	HOMO −1 → LUMO +1 (0.22)
					HOMO −2 → LUMO (0.20)
					HOMO −3 → LUMO (0.32)
					HOMO −3 → LUMO +1 (0.20)
					HOMO −4 → LUMO +1 (0.22)
22 (S_{10})	10.91	0.071	6.27	197.9	HOMO → LUMO (0.28)
					HOMO −4 → LUMO (0.37)
					HOMO −4 → LUMO +1 (0.30)
28 (S_{13})	17.83	0.066	6.38	194.3	HOMO → LUMO (0.61)
					HOMO −2 → LUMO (0.11)
					HOMO −3 → LUMO +1 (0.10)
					HOMO −4 → LUMO (0.16)
37 (S_{18})	4.53	0.449	6.74	183.8	HOMO −1 → LUMO +4 (0.23)
					HOMO −2 → LUMO +4 (0.20)
					HOMO −3 → LUMO +4 (0.41)
					HOMO −4 → LUMO +3 (0.29)
47 (S_{23})	15.01	0.052	7.07	175.4	HOMO → LUMO +4 (0.45)
					HOMO −4 → LUMO +4 (0.42)

[a] The excited states correspond exactly as listed in the AM1/sum-over-states output.

Inspection of these excited states reveals that several of the transitions involve charge transfer from the amino group and the amino-substituted aryl ring to the unsubstituted aryl rings. Again, some of the transitions involve transfer of charge from the unsubstituted aryl rings to the amino-substituted aryl ring and from the phosphoryl oxygen to the aryl rings.[86] However, *none* of the transitions involve charge transfer from the amino donor to the phosphoryl moiety. Thus, the large hyperpolarizability $||\beta||$ arises from transitions mainly involving the transfer of charge from the amino group and the amino-substituted aryl ring to the unsubstituted aryl rings and, perhaps, from the unsubstituted aryl rings to the amino-substituted aryl ring.

The explanation for the decreasing values of $||\beta||$ for the di- and trisubstituted compounds **2a** and **3a** now becomes apparent and can be effectively visualized by referring to Figure 8. With one para amino substituent in **1a** (Figure 8a), the major transitions involve charge transfer from the amino substituent and the amino-substituted aryl ring to the two unsubstituted aryl rings.

(86) Earlier studies of the electronic absorption spectra of substituted arylphosphine oxides address the issue of conjugation between the aryl rings. For heading references, see: (a) Schiemenz, G. P.; Nielsen, P. *Phosphorus Sulfur* **1985**, *21*, 267–276. (b) Schiemenz, G. P.; Röhlk, K. *Chem. Ber.* **1971**, *104*, 1722–1727. (c) Cheng, C. Y.; Shaw, R. A. *J. Cryst. Spectrosc. Res.* **1987**, *17*, 331–348.

(87) Hyperpolarizability $||\beta||$ was computed using 12 active orbitals (PECI = 12). For compound **1a**, our results establish that $||\beta||$ converges satisfactorily when utilizing 10 or more active orbtials. All 12 active orbitals are shown in the molecular orbital analyses depicted in Figure 7 and Table 5.

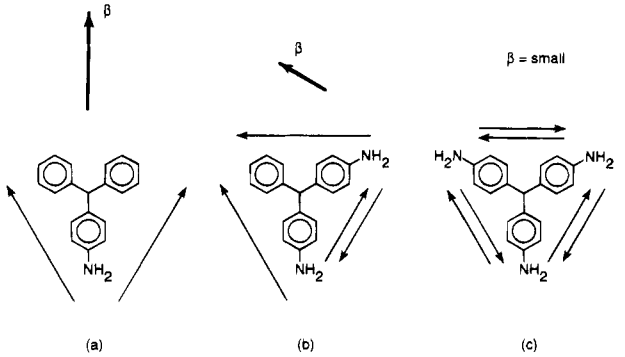

Figure 8. Schematic illustration of the orientation of β (solid arrow) in (a) **1a**, (b) **2a**, and (c) **3a** (as viewed down the P=O bond).

These contributions result in a large β (bold arrow). With two para amino substituents in **2a** (Figure 8b), the charge-transfer transitions among the two amino-substituted aryl rings and the single unsubstituted aryl ring become more heavily mixed, resulting in a decreased β (bold arrow). With three para amino substituents in **3a** (Figure 8c), the major transitions cancel (almost) completely, resulting in a small β. Our explanation for the decrease in β for the series **1a**, **2a**, and **3a** implies that the octupolar contributions in **2a** and **3a** are not large.[27] Octupolar contribution could, however, explain why β does not vanish. The MO analyses for **2a** and **3a** are completely consistent with the fact that the transitions from amino group to aryl ring and from aryl ring to aryl ring are significantly reduced in these molecules. Since the mechanism responsible for $||\beta||$ is charge transfer from either the amino or the hydroxy donor in **1a** and **1b** to the aryl substituents on the phosphoryl moiety but *not* to the phosphoryl moiety itself, introduction of additional electron-donating substituents in **2a**, **2b**, **3a**, or **3b** results in a decreased hyperpolarizability.

Table 2 lists the angle, $\theta_{\beta\mu}$, between the dipole moment (μ) and hyperpolarizability (β) vectors for **1**–**9** obtained from the calculations. For triphenylphosphine oxide **6**, $\theta_{\beta\mu}$ is 165–180°. This large angle indicates that β and μ are nearly coincident but antiparallel; consequently, β_μ essentially equals $||\beta||$. Substitution of **6** with amino or hydroxyl groups affects the orientation of β more strongly than μ, as evidenced by the smaller angle, $\theta_{\beta\mu}$, between μ and β for **1**–**3**. In each case, μ lies primarily along the P=O bond. As β becomes increasingly orthogonal to μ, β_μ diminishes. The amino-substituted compounds possess $\theta_{\beta\mu}$ close to 90° (Table 2), indicating that β and μ are nearly orthogonal in these molecules. As a result, β_μ is very small. As such, the calculations predict that experimental EFISH measurements, which determine β_μ directly (if the dipole moment μ is known), will not accurately reflect the intrinsic hyperpolarizabilities ($||\beta||$) of the phosphine oxides **1**–**3**.

To address the problem of orthogonal μ and β, we substituted (4-aminophenyl)diphenyl phosphine oxide (**1a**) with electronegative $-CF_3$ or $-NO_2$ substituents. We reasoned that the two $-CF_3$ substituents in (4-$NH_2C_6H_4$)(4′-$CF_3C_6H_4$)$_2$P=O (**5**) would not significantly perturb the intrinsic hyperpolarizability of **1a** due to the lack of resonance interactions of the $-CF_3$ groups. The net effect of substitution would simply be to tip the dipole moment vector of **1a** away from the P–O bond axis and in the direction of the maximum hyperpolarizability. Although the calculations predict a decrease in $||\beta||$ upon $-CF_3$ substitution (28.7×10^{-30} cm^5 esu^{-1} for **1a** vs 17.0×10^{-30} cm^5 esu^{-1} for **5**), they do predict an increase in β_μ (2.0×10^{-30} cm^5 esu^{-1} for **1a** vs 13.5×10^{-30} cm^5 esu^{-1} for **5**). We reasoned not only that the $-NO_2$ substituent in (4-$NH_2C_6H_4$)(4′-$NO_2C_6H_4$)PhP=O (**4**) would tip the dipole moment in the direction of maximum hyperpolarizability but also that it might actually serve to increase the hyperpolarizability by virtue of lowering the energy of the charge-transfer excited states. As in the case of the $-CF_3$ substituent, the calculations predict a decrease in $||\beta||$ upon $-NO_2$ substitution (28.7×10^{-30} cm^5 esu^{-1} for **1a** vs 19.7×10^{-30} cm^5 esu^{-1} for **4**), but they predict an increase in β_μ (2.0×10^{-30} cm^5 esu^{-1} for **1a** vs 11.2×10^{-30} cm^5 esu^{-1} for **5**).

The experimental EFISH measurements of compounds **1**–**3** reveal only moderate values of β_μ (Table 2), in fairly good agreement with the β_μ values calculated by the AM1/sum-over-states method. As such, these EFISH β_μ values are considerably less than the calculated intrinsic hyperpolarizabilities, $||\beta||$, and it is evident that the experimental EFISH measurements probably do not accurately reflect the intrinsic molecular hyperpolarizability $||\beta||$. Nevertheless, both computational and experimental results suggest that the intrinsic nonlinearity of the donor/acceptor combination of NH_2/P=O in **1a** is comparable to that of 4-nitroaniline (**9**). From a practical perspective, however, phosphine oxides **1a** and **1b** have a serious drawback: β and μ are not coincident. For this situation, the problem of favorably aligning the molecules along the direction of the hyperpolarizability becomes increasingly complicated. Alignment in the direction of the dipole moment does not achieve alignment in the direction of the hyperpolarizability if $\theta_{\beta\mu}$ is large. This is exactly the case in the EFISH measurements of **1**–**3**, where the applied voltage aligns the molecules in the direction of the dipole moment, but not necessarily in the direction of β. The EFISH measurements demonstrate that substitution of (4-$NH_2C_6H_4$)Ph_2P=O (**1a**) by electronegative substituents to produce (4-$NH_2C_6H_4$)(4′-$NO_2C_6H_4$)PhP=O (**4**) and (4-$NH_2C_6H_4$)(4′-$CF_3C_6H_4$)$_2$P=O (**5**) increases β_μ, as predicted by the calculations (Table 2). Despite this increase, the absolute magnitudes of β_μ remain small because **4** and **5** still possess moderate values of $\theta_{\beta\mu}$.

The high thermal stability of **1a** (mp = 246 °C) and **1b** (mp = 242 °C) compared to triphenylphosphine oxide **6** (mp = 156 °C) suggests a large degree of intermolecular hydrogen bonding in **1a** and **1b**. Compounds **2a**, **2b**, and **3b** all display a substantial increase in the melting point as well. X-ray crystal structures obtained for compounds **1a**, **1b**, **2b**, and **3b** confirm extensive intermolecular hydrogen bonding in the solid state. In fact, monoaminophosphine oxide **1a** and monohydroxyphosphine oxide **1b** both crystallize in noncentrosymmetric space groups (*Cc* and *Pca*2_1, respectively). Powder SHG results reveal that **1a**, **1b**, and **5** are capable of SHG in the solid state (Table 3). However, for **1a**, the structure is essentially centrosymmetric, with only small distortions due to the intermolecular hydrogen bonding removing the center of symmetry. As such, the powder SHG intensity is weak (0.01 × urea).

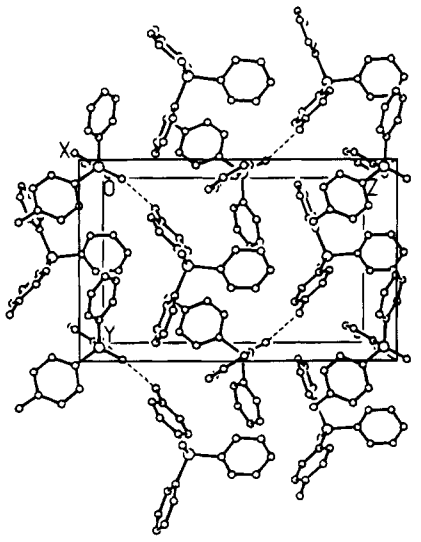

Figure 9. X-ray crystal packing diagram (ball and stick, hydrogen atoms omitted) for (4-hydroxyphenyl)diphenylphosphine oxide (**1b**). The dashed lines indicate hydrogen bonding.

A similar situation arises in compound **1b**, with the exception that the distortions from a centrosymmetric structure are more pronounced, resulting in a powder SHG intensity of the same order of magnitude as urea. Figure 9 shows the crystal packing arrangement of **1b**, illustrating the nearly centrosymmetric alignment of molecules. Interestingly, the powder SHG intensity of the *nearly centrosymmetric* compound **1b** is similar to that obtained from urea, suggesting that phosphine oxide **1b** probably does possess a moderate to large molecular hyperpolarizability. No X-ray data are available for phosphine oxide **5**.

Summary

Both AM1/finite field and AM1/sum-over-states calculations predict a moderate molecular hyperpolarizability for (4-aminophenyl)diphenylphosphine oxide (**1a**). This prediction is surprising, because the phosphine oxide moiety is a weaker electron acceptor than substituents traditionally used in NLO materials. Molecular orbital analysis indicates that the hyperpolarizability arises not by charge transfer from the $-NH_2$ group to the P=O moiety but instead by charge transfer from the $-NH_2$ group and the substituted aryl ring to the unsubstituted aryl rings. Compounds **1**–**3** form highly crystalline solid-state structures characterized by extensive intermolecular hydrogen bonding and high thermal and mechanical stability. These properties could be exploited by using these materials as cocrystallization aids for solid-state optical materials. Most importantly, compounds **1**–**3** display excellent transparency in the visible and near-UV spectral regions. This is an important characteristic for certain applications of second-order nonlinear optical materials (e.g., frequency doubling of diode lasers to the near-UV).[9] In comparing (4-aminophenyl)diphenylphosphine oxide (**1a**) with 4-nitroaniline (**9**), a conventional nonlinear optical material of similar size, it is significant that the intrinsic hyperpolarizability of **1a** is comparable to that of **9**, while the onset of electronic absorption for **1a** occurs at *ca. 100 nm shorter wavelength* than **9**. These results have important ramifications in designing efficient materials with better optical transparency in the visible and near-UV spectral ranges. Although **1a** possesses a relatively large intrinsic hyperpolarizability, it suffers from the severe practical limitation that μ and β are nearly orthogonal. This leads to a very small value for β_μ. The electronegative $-CF_3$ and $-NO_2$ substituents of phosphine oxides **4** and **5** force μ and β to be more nearly collinear, resulting in an increase in β_μ.

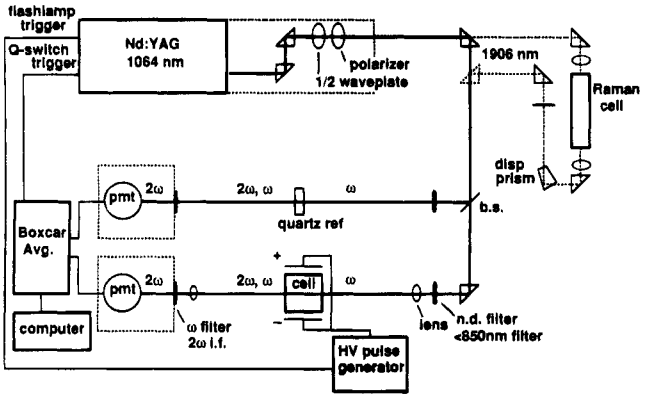

Figure 10. Schematic diagram of the EFISH experiment.

Our results concerning the nonlinear optical response of phosphine oxides demonstrate the need for continuing, exploratory studies to further define the relationship between molecular structure and hyperpolarizability. In particular, the results of this investigation would not have been anticipated within the context of the "two-level model". We emphasize that the two-level model may be a useful predictive tool for *certain classes* of second-order nonlinear optical materials, *but not all classes*. The phosphine oxides serve as a case in point. The two-level model does not necessarily provide insight for the discovery of *new paradigms* in the design of molecular nonlinear optical materials.

Experimental Section

Materials. The syntheses of phosphine oxides **1**–**6** are described elsewhere.[49a] 4-Nitroaniline (**9**, Aldrich) was purified by column chromatography (SiO_2) and then recrystallized prior to use. *p*-Dioxane was refluxed with HCl, dried over KOH, and distilled from Na.[88] $CHCl_3$ was shaken with concentrated H_2SO_4, washed with water, dried over $CaCl_2$, and distilled.[88] In practice, we obtained comparable results when using $CHCl_3$ from a freshly opened bottle.

Electric-Field-Induced Second-Harmonic (EFISH) Generation. A schematic diagram of the EFISH experiment is shown in Figure 10. The experiment utilizes a Continuum Model NY-61 Q-switched Nd:YAG laser operating at a fundamental wavelength of 1064 nm (10 Hz repetition rate, 6 ns pulse width). The laser beam is attenuated and vertically (s) polarized using the combination of a half-waveplate (Special Optics Model 8-8015-1/2) and a polarizer (Special Optics Model 7-1210-M-V). The beam can be further attenuated using neutral density filters (Schott). Schott RG850 filters remove scattered light from the flash lamps and second-harmonic light generated from the optical components (e.g., half-waveplate). Part of the fundamental laser beam is split off using a plate beamsplitter (Melles Griot Model 03BTF015), and passed through a Z-cut quartz reference crystal (Special Optics) in order to monitor and divide out fluctuations in the laser power.

A beam of 0.8 mJ average power is focused into the solution cell using a 35 cm focal length lens (Esco Products Model A510120). An Instrument Research Co. Model 994A high-voltage pulse generator supplies a 10 μs, 9 kV pulse across

(88) Gordon, A. J.; Ford, R. A. *The Chemist's Companion*; Wiley: New York, 1972; pp 432–433.

the solution cell to orient the solute molecules. This allows observation of second-harmonic generation at 532 nm. The fundamental at 1064 nm is filtered from the transmitted beam using Schott KG-3 filters and 532 nm interference filters (Corion Model P10532-F, 10 nm bandwidth). The second harmonic signals at 532 nm generated from the sample solution and from the quartz reference crystal are detected with Hamamatsu Model R928 high-gain photomultiplier tubes. Stanford Research Systems Model SR250 gated integraters are used to collect the signals, which are then sent to a Stanford Research Systems Model SR245 analog-to-digital converter and transferred to a laboratory computer. The computer averages over several laser pulses and takes the ratio of the sample to reference signals, which are then stored to a data disk. Alternatively, measurements can be performed at 1906 nm, the first Stokes output obtained from pumping a high-pressure hydrogen cell with the 1064 nm Nd:YAG output.

We perform a series of preliminary checks to verify that the observed signal is in fact electric-field-induced SHG. First, we establish that the harmonic intensity ($I_{2\omega}$) is proportional to the square of the applied voltage (E_0), $I_{2\omega} \propto E_0^2$. Second, we establish that the harmonic intensity is proportional to the square of the fundamental input power (I_0), $I_{2\omega} \propto I_0^2$. Finally, we verify that the observed signal is not due to fluorescence by observing the disappearance of the signal upon rotation of the interference filter.

The wedged-shaped solution cell is comprised of two highly polished BK-7 optical windows (Optical Spectrum Technology) of dimension 50 mm × 10 mm × 2 mm and two highly polished stainless steel electrodes (Figure 3). The angle between the optical windows was measured using a HeNe laser to be 0.974°.[89] The electrodes are placed above and below the wedge-shaped solution compartment. Glass tubes attached to the cell via holes drilled into the top electrode allow for easy filling and cleaning of the cell. The cell is bonded and permanently sealed using a fluorinated silicone adhesive (General Electric, FRV 1106). The cell is mounted on a kinematic table (Newport Model MM-2) which in turn is mounted on the combination of a telescoping post (Newport Model VPT-03), a rotation stage (Newport Model RSX-1), and a basic translation stage (Newport Model TSX-1A), allowing for fine adjustment of the cell in all dimensions. This entire assembly is mounted on a low-profile translation stage (Newport Model 421-OMA) driven by a motorized actuator (Newport Model 850B-1) and motion controller (Newport Model PMC-100). The solution cell is thus carefully aligned in the focus of the laser beam. Synchronizing a high-voltage pulse across the solution cell with the laser pulse results in Maker fringes upon translation of the cell across the laser beam. The fringe pattern results from the path length variation Δl of the laser beam through the cell introduced by translating the cell in the y direction (Figure 3a). Figure 3b shows typical Maker fringe data for 4-nitroaniline (**9**) in *p*-dioxane. The Maker fringe pattern is fit to eq 23 using a nonlinear least-squares fitting program based on a Marquardt algorithm.

(89) Murty, M. V. R. K.; Shukla, R. P. *Opt. Eng.* **1979**, *18*, 177–180.

Acknowledgment. We thank the National Science Foundation for support through the Presidential Young Investigator Program (CHE-8957529). We gratefully acknowledge matching funding from the 3M Corp., DuPont Corp., and Rohm and Haas Corp. We express our appreciation to Dr. Gary T. Boyd (3M Corp.) and to Professor Kenneth D. Singer (Case Western Reserve University) for invaluable advice concerning the assembly of the EFISH experiment, to Dr. Lou J. Trigas (3M Corp.) for helpful discussion concerning the design of the capacitance cell and the determination of solution dielectric constants, and to Dr. Daniel A. Higgins and Professor Robert M. Corn for helpful discussion concerning the design of our optical system. We are grateful to Professor Tim Clark (Erlangen) for providing his VAMP program and to Professor Stephen F. Nelsen for insightful comments. We thank Dr. Douglas R. Powell for the X-ray crystallographic analyses. Departmental computing facilities were purchased with funds provided by the National Science Foundation (CHE-9007850). K.L.K. thanks the Amoco Corp. for a graduate fellowship. C.M.W. thanks the Department of Education for a graduate fellowship.

Supplementary Material Available: Table of physical constants used in the analysis of EFISH experiment (1 page). This material is contained in many libraries on microfiche, immediately follows this article in the microfilm version of the journal, and can be ordered from the American Chemical Society. Ordering information is given on any current masthead page.

CM940520R